red line in Figure 2 indicates the lowest possible temperature of the RCM system, which is set to be 408 K. When heating the RCM to 420 K, the temperature readings of all temperature-measuring points on mixing tank, reaction chamber, and manifold are within 410–423 K. Therefore, we select 408 K as the lowest temperature limit to ensure no condensation. This also means that when preheating the mixture before experiments, we have chosen a margin of 12 K and to ensure that the partial pressure of each surrogate component is still lower than its saturated vapor pressure at 408 K. From Figure 2 it can be observed that in this temperature range, when designing the test matrix, the top five components require attentions to avoid condensation are NEI, *n*-octadecane (NOD), *n*-hexadecane (NHXD), *iso*-cetane (HMN), and 1-methylnapthalene (1-MN), because their saturated vapor pressures are relatively lower.

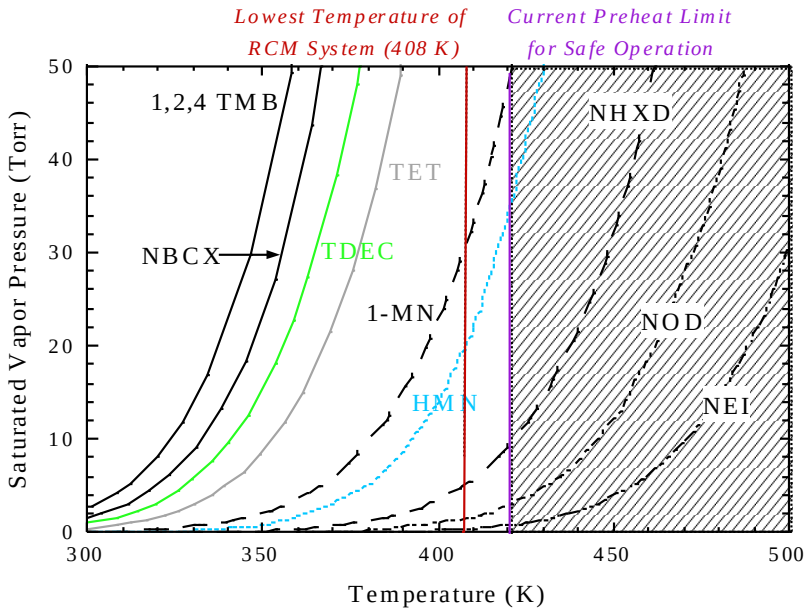

Figure 2: Plot showing the saturated vapor pressures of CRC surrogate components as a function of temperature.

2.1 Test Matrix Design and Limitations

The test conditions investigated in the current study are outlined in Table 2, which have been designed to show the effect of pressure, fuel loading, and oxygen concentration on the ignition delay time, and to cover wide range of temperature windows in the Arrhenius plot. The equivalence ratios (ϕ), molar percentages of mixture constituents (X_i), and compressed pressures (P_C), which is the pressure at the end of compression, have been specified in Table 2, and for each set of (ϕ, X_i, P_C), the temperature windows covered in Arrhenius plots for experimental ignition delays, including low temperature regime (LTR), negative temperature coefficient (NTC) regime, and intermediate temperature regime (ITR), are also specified. The mixture conditions varying from fuel lean, stoichiometric, to fuel rich are investigated herein in order to provide data at wider equivalence ratio range for chemical kinetic model development and validation. From Table 2, it is noted that not all temperature windows can be covered in Arrhenius plots for some test conditions, which is because of the limitations such as partial pressure, ignition delay time, and exothermicity in the compression stroke. These limitations are explained in the following, with V0b as an example, as it includes the highest amount of heavy component (i.e., *n*-octadecane of 23.5% mole percentage) compared with the other three CRC surrogates. Table 3 further summarizes the experimental conditions of V0b and CFA#2, as well as the limitations for not being able to cover the entire curve of Arrhenius plot for V0b.

The compressed temperature (T_C), namely the gas temperature at the end of compression, is used as the reference temperature in reporting the present RCM data, and is deduced from the measured pressure trace by using the assumption of "adiabatic core hypothesis" [6]. Under this hypothesis, it is assumed that the heat loss from the core volume of the reaction chamber only occurs in a thin boundary layer near the wall, and the central core region is adiabatic by modeling the heat loss as an effective reduction in the compression ratio [7,8]. Thus, the compressed temperature can be calculated by $\ln\left(\frac{P_C}{P_0}\right) = \int_{T_0}^{T_C} \frac{\gamma}{T(\gamma-1)} dT$, where P_0 is the initial pressure, T_0 is the initial temperature, and γ is the temperature-dependent specific heat ratio.

Table 2: Test conditions for CFA#2 diesel and CRC surrogates.

ϕ	Oxidizer	X_{fuel} (%)	X_{O2} (%)	X_{N2} (%)	P_C (bar)	Regime Covered for CFA#2	Regime Covered for V0a	Regime Covered for V0b	Regime Covered for V1	Regime Covered for V2
0.5	Air	0.51	20.9	78.59	10	LTR/NTC/ ITR	LTR/NTC/ ITR	LTR/NTC/ ITR	LTR/ITR	LTR/NTC/ ITR
0.69	Diluted	0.51	15.12	84.37	10	LTR/NTC/ ITR	LTR/NTC/ ITR	LTR/NTC/ ITR	LTR/NTC/ ITR	LTR/NTC/ ITR
1.02	Diluted	0.51	10.24	89.25	10	LTR/NTC/ ITR	LTR/NTC/ ITR	-	NTC/ITR	LTR/NTC/ ITR
1.02	Diluted	0.51	10.24	89.25	15	LTR/NTC/ ITR	LTR/NTC/ ITR	LTR/ITR	NTC/ITR	LTR/NTC/ ITR
2.0	Diluted	0.51	5.12	94.37	20	LTR/NTC/ ITR	LTR/NTC/ ITR	ITR	LTR/NTC/ ITR	LTR/NTC/ ITR
0.7	Diluted	0.36	10.47	89.17	15	LTR/NTC/ ITR	LTR/NTC/ ITR	NTC/ITR	LTR/NTC/ ITR	LTR/NTC/ ITR

Table 3: V0b test matrix and limitations, along with the test conditions of CFA#2.

ϕ	Oxidizer	X_{fuel} (%)	X_{O2} (%)	X_{N2} (%)	P_C (bar)	Regime Covered for CFA#2	Regime Covered for V0b	Limitation
0.5	Air	0.51	20.9	78.59	10	LTR/NTC/ITR	LTR/NTC/ITR	-
0.69	Diluted	0.51	15.12	84.37	10	LTR/NTC/ITR	LTR/NTC/ITR	-
1.02	Diluted	0.51	10.24	89.25	10	LTR/NTC/ITR	-	IDT
1.02	Diluted	0.51	10.24	89.25	15	LTR/NTC/ITR	NTC/ITR	P_{V0b}
1.02	Diluted	0.51	10.24	89.25	20	LTR/ITR	-	P_{V0b}
2.0	Diluted	0.51	5.12	94.37	20	LTR/NTC/ITR	ITR	P_{V0b}
0.7	Diluted	0.36	10.47	89.17	15	LTR/NTC/ITR	NTC/ITR	IDT
0.35	Air	0.36	20.9	78.74	15	-	LTR/ITR	Exothermicity
0.35	Air	0.36	20.9	78.74	10	-	ITR	IDT

2.1.1 Partial Pressure of V0b (P_{V0b}) Consideration

As mentioned earlier, when preparing a fuel/oxidizer mixture, we always ensure that the partial pressure of each component in V0b is less than half of its corresponding saturated pressure at the preheat temperature of 420 K. It is noted that the highest fuel molar percentage (X_{fuel}) in diesel autoignition study is set to be 0.51%. Therefore, when heating from room temperature to 420 K, the highest pressure of the test mixture in the mixing tank can be 1280 Torr, with the saturated pressure and partial pressure of *n*-octadecane to be 3.1 Torr and 1.54 Torr, respectively. When P_C=15 bar, the required P_0 for data points in the LTR and NTC regime is typically in the range of 900–1700 Torr. Hence, only a small part of NTC and ITR can be covered for X_{fuel}=0.51% at P_C=15 bar, starting at the end-of-compression temperature of T_C=780 K with P_0=1050 Torr, resulting in the data points in the LTR not available for X_{fuel}=0.51% at P_C=15 bar. When P_C=20 bar, the required P_0 for data points in the LTR and NTC regime is typically in the range of 1300–2200 Torr. As a result, experimental data of V0b are not available for test conditions with X_{fuel}=0.51% at P_C=20 bar.

2.1.2 Ignition Delay Time (IDT) Consideration

We choose not to report data points that have total ignition delay times longer than 100 ms because we are concerned about the effect of residual vortex (if any) on the core region of reaction chamber after long duration that may lead to inhomogeneity. For ϕ=1.02 with X_{fuel}=0.51% at P_C=10 bar, the ignition delay data of V0b are not available because based on the autoignition results of V0b at ϕ=0.69 and P_C=10 bar, as well as the CFA#2 result at ϕ=1.02 and PC=10 bar, it can be inferred that data points of V0b in both the LTR and NTC regime will exceed 100 ms.

2.1.3 Exothermicity during the Compression Stroke Consideration

For ϕ=0.35 with X_{fuel}=0.36% at P_C=15 bar, the NTC regime is not available because of some exothermicity in the compression stroke is noted from the pressure trace comparison of reactive experiment and its nonreactive counterpart (obtained by replacing O_2 with N_2 in the test mixture). Figure 3 shows an example of pressure trace with exothermicity near the end of the

compression stroke, marked by a red rectangle, by comparing the reactive and nonreactive experimental pressure traces with the same initial pressure and machine settings. It can be observed that there is a discrepancy near the end of compression, showing that the reactive experiment can reach higher pressure and temperature at the end of compression as compared to the nonreactive experiment. Therefore, those ignition delay data with exothermicity during the compression stroke are not included in the Arrhenius plots.

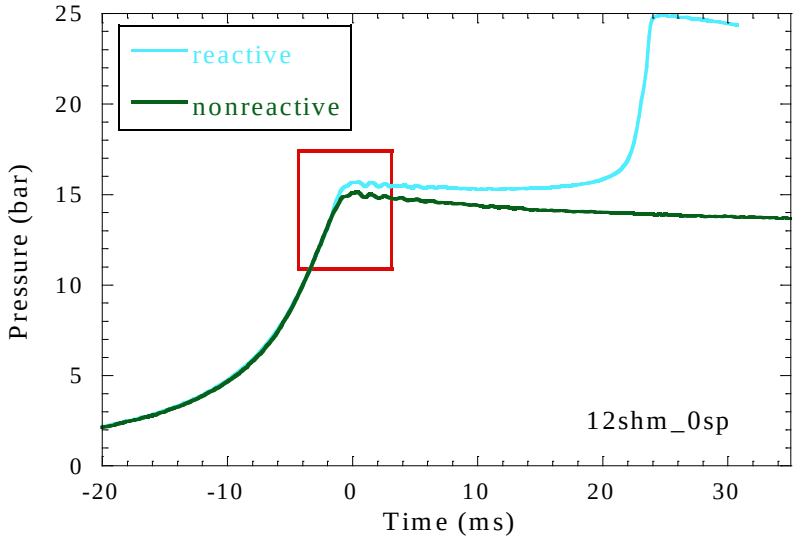

Figure 3: Comparison of experimental reactive and nonreactive pressure traces of V0b/oxidizer mixtures of ϕ=0.35 in air at P_C=15 bar with the same initial pressure and machine settings. The compressed temperature based on the nonreactive experiment is T_C=809 K.

2.2 Vaporization check of CFA#2, V0a, and V0b

The vaporization checks have been conducted to ensure that fuel injected into the mixing tank have vaporized completely. Theoretically, Table 4 shows the saturated vapor pressures and partial pressures of the five components mentioned earlier that have lower saturated vapor pressures at preheat temperature at 420 K and 408 K. This table is calculated based on the highest pressure in the mixing tank of 1280 Torr at 420 K with the highest fuel molar percentage of 0.51%. It can be observed that the partial pressure of each component is less than half of its corresponding saturated pressure at 420 K, and is also less than its corresponding saturated pressure at 408 K.

Table 4: Saturated vapor pressures of some components at 420 K and 408 K and their partial pressures.

ϕ	Saturated Vapor Pressure at preheat 420 K (Torr)	Saturated Vapor Pressure at preheat 408 K (Torr)	Maximum Partial Pressure (Torr)
1-MN	49.16	31.42	1.39
HMN	33.28	20.02	2.39
NHXD	9.03	5.06	1.83
NOD	3.1	1.66	1.55
NEI	1.12	0.57	0.05

Experimentally, the vaporization checks were carried out by preheating the mixing tank to 420 K, then injecting a known mass of fuel and recording the time history of the pressure inside the tank. The pressure calculated from the ideal gas law for the same known fuel mass was set as a reference, which assumes that the fuel has completely vaporized in the mixing tank. The vaporization check results of CFA#2, V0a, and V0b are shown in Figure 4, with the error bars indicating that the full scale uncertainty of the pressure transducer is 0.05%, thus resulting in an uncertainty of ±2.6 Torr. Note that V0a and V0b are respectively the most and least volatile surrogates among the four CRC surrogates. In addition, the fuel masses injected into the preheated mixing tank for the results shown in Figure 4 are 1.64 g, 1.85 g, and 0.93 g for CFA#2, V0a, and V0b, respectively, which are equal to or even more than the mass of fuel in the highest fuel loading conditions planned in the present RCM experiments. It is seen from Figure 4 that for diesel and surrogates, more than 85% of the reference pressure was reached instantly after the liquid fuel was injected into the tank. After that, the pressure reached to ~95% of the expected value rapidly and this remained unchanged for more than an hour. These vaporization checks therefore demonstrate that the uncertainty of fuel partial pressure in the mixing tank is consistently ~5%.

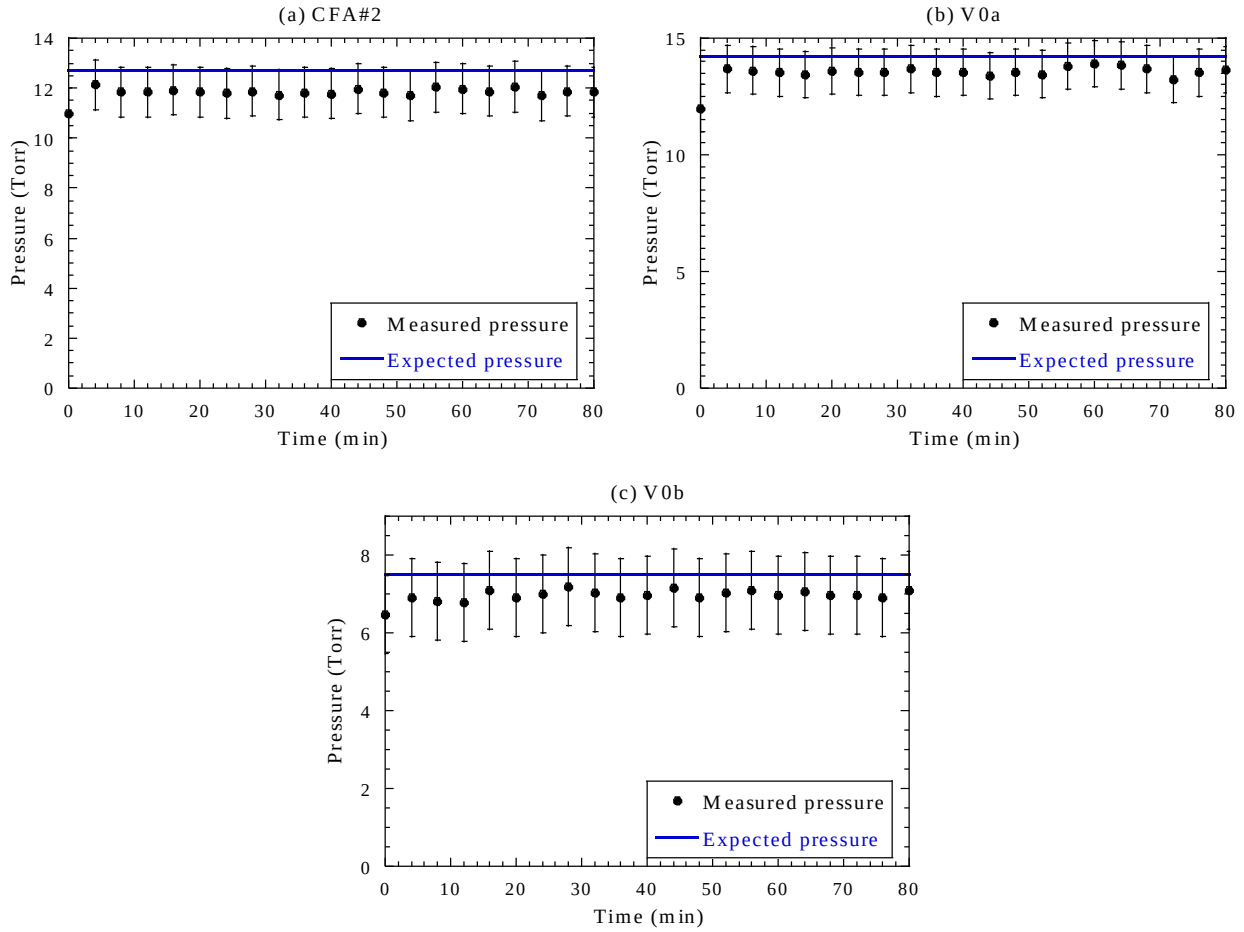

Figure 4: Measured time-history of pressure in the mixing tank after liquid fuel injection for (a) CFA#2, (b) V0a, and (c) V0b. The pressure calculated from the ideal gas law assuming complete vaporization is also shown as a reference.

2.3 Ignition Delay Definition and Experimental Repeatability

Figure 5(a) shows a representative pressure trace of V2/oxidizer at P_C=20 bar, T_C=699 K, and ϕ=1.02 with dilution, demonstrating the definitions of ignition delay times used in this study. The end of compression point was regarded as the starting point of ignition delay time, which is set as t=0 ms. In Figure 5(a), τ_1 indicates the first-stage ignition delay time and τ indicates the total ignition delay time, with both of them being identified based on the respective local maximum of the time derivative of the pressure trace. The non-reactive pressure trace of the same experimental condition has also been shown in Figure 5(a) as a reference. For each reactive set of P_C and T_C, the corresponding non-reactive pressure trace is measured by replacing oxygen with nitrogen to characterize the heat loss effect on the ignition process and to verify that no heat release has occurred during the compression stroke. Four to five consecutive runs were taken for each experimental condition to ensure data repeatability, which can be seen in Figure 5(b), with representative pressure traces of V1/oxidizer at P_C=20 bar, T_C=840 K, and ϕ=2.0 with dilution. The typical scatter was found to be less than 10% of the reported ignition delay value, which is closest to the mean of the consecutive runs.

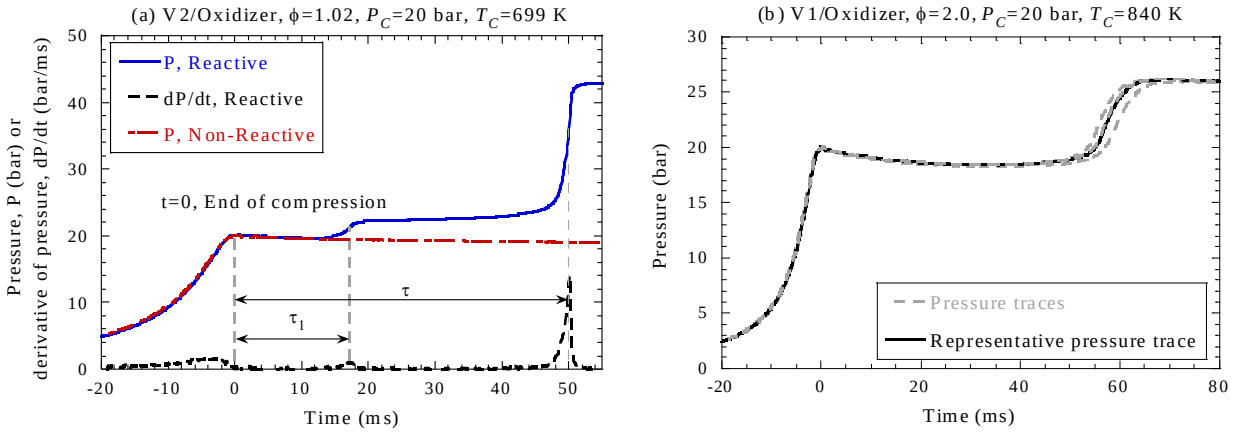

Figure 5: (a) Definitions of first-stage and total ignition delay times, and the corresponding non-reactive pressure trace of V2/oxidizer at P_C=20 bar, T_C=699 K, and ϕ=1.02 with dilution. (b) Pressure traces of V1/oxidizer at P_C=20 bar, T_C=840 K, and ϕ=2.0 with dilution showing the experimental repeatability of the current study.

The ignition delay data scatters of CFA#2 diesel and the four CRC surrogates are further compared to provide additional checking on the potential fuel condensation issue. Table 5 demonstrates the scatter checks for CFA#2 and CRC surrogates at the same representative conditions. From Mueller et al. [3], the sequence of surrogates that have higher mole fraction of *n*-octadecane is V0a>V2>V1>V0b. If condensation were to occur in experiments of surrogates with more heavy components, the scatters are expected to increase with increasing heavy component mole fraction in the surrogate. However, the scatters shown in Table 5 are not increasing as the amount of heavy component increases. Table 6 further shows the scatter checks for CFA#2 diesel and CRC surrogates at different temperatures representing LTR, NTC regime, and ITR. It is noted that the scatter of V0b at T_C=840 K is not shown in Table 6, which is because this data point at ϕ=0.5 and P_C=10 bar is not available due to exothermicity during the compression stroke. Again, for CFA#2 diesel and each surrogate, the scatters are not decreasing as temperature increases. Thus, it can be inferred from both Table 5 and Table 6 that there is no apparent condensation issue in our RCM experiments.

Table 5: Ignition delay scatter checks for CFA#2 diesel and CRC surrogates at the same representative conditions.

ϕ	P_C (bar)	T_C (K)	Scatter of CFA#2	Scatter of V0a	Scatter of V2	Scatter of V1	Scatter of V0b
0.5	10	702	3.1%	1.6%	7.9%	4.7%	2.2%
2.0	20	840	5.1%	8.2%	6.7%	3%	6%
2.0	20	920	4.2%	4.9%	8.3%	2.5%	1.2%

Table 6: Ignition delay scatter checks at varying temperatures for CFA#2 diesel and CRC surrogates.

	ϕ=1.0 P_C=20 bar	ϕ=1.0 P_C=20 bar	ϕ=1.0 P_C=20 bar	ϕ=0.69 P_C=10 bar	ϕ=0.5 P_C=10 bar
T_C (K)	Scatter of CFA#2	Scatter of V0a	Scatter of V2	Scatter of V1	Scatter of V0b
702	4.6%	4.6%	4.8%	2.1%	2.2%
840	5.1%	8.2%	6.7%	8.7%	–
920	4.2%	4.9%	8.3%	4.5%	6.3%

3. Results and Discussion

3.1 Effects of Pressure, Fuel Loading, and Oxygen Concentration on IDT

Figure 6 shows the effect of varying pressure on total and first-stage ignition delays of the four CRC surrogates. It can be observed that both the total ignition delays and first-stage ignition delays decrease with increasing pressure, but the effect of pressure on first-stage ignition delays is less pronounced. For V1 at ϕ=1.02, it is seen from Figure 6(c) that only part of V1 data points in the LTR are reported. This is because for P_C=10 bar, the ignition delay times in the LTR are more than 100 ms; for P_C=15 bar, on the other hand, the total pressure in the mixing tank at 420 K cannot provide sufficient initial pressure to reach the target P_C, which is the limitation of partial pressure mentioned earlier.

Figure 7 shows the effect of varying fuel loading on ignition delays for the four CRC surrogates at P_C=15 bar. It can be observed that the total ignition delays are seen to decrease with increasing equivalence ratio (fuel loading) from ϕ=0.7 to ϕ=1.02, but there is not much fuel loading effect observed on first-stage ignition delays.

Figure 8 further shows the effect of oxygen concentration on the total and first-stage ignition delays of the four CRC surrogates at P_C=10 bar. It is seen that lowering the oxygen mole fraction increases both the total and first-stage ignition delays, and this effect on total ignition delays is still more pronounced.

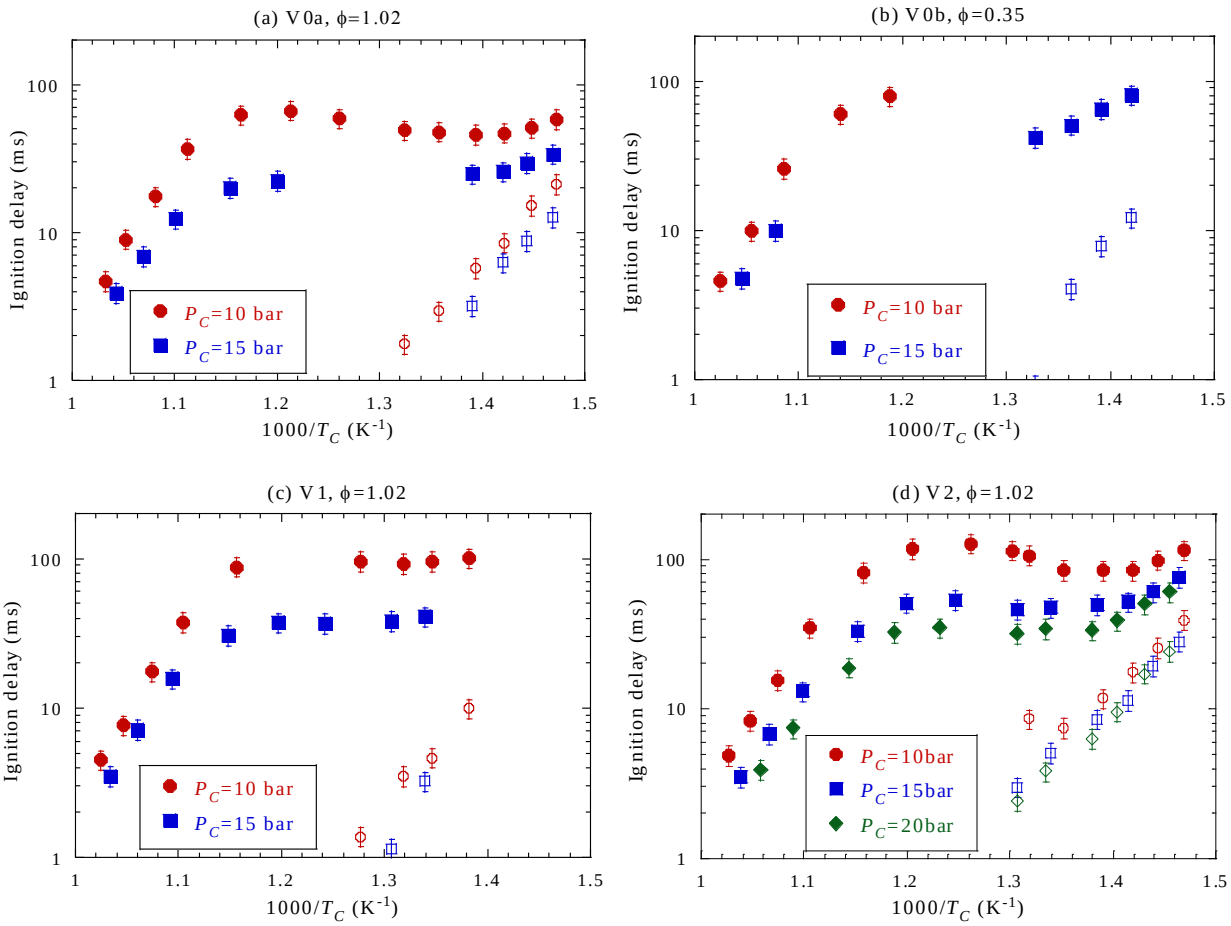

Figure 6: Effect of compressed pressure on total and first-stage ignition delays for (a) V0a/oxidizer mixtures at ϕ=1.02 with dilution, (b) V0b/oxidizer mixtures at ϕ=0.35 in air, (c) V1/oxidizer mixtures at ϕ=1.02 with dilution, and (d) V2/oxidizer mixtures at ϕ=1.02 with dilution. Filled symbols correspond to total ignition delays and open symbols correspond to first-stage ignition delays.

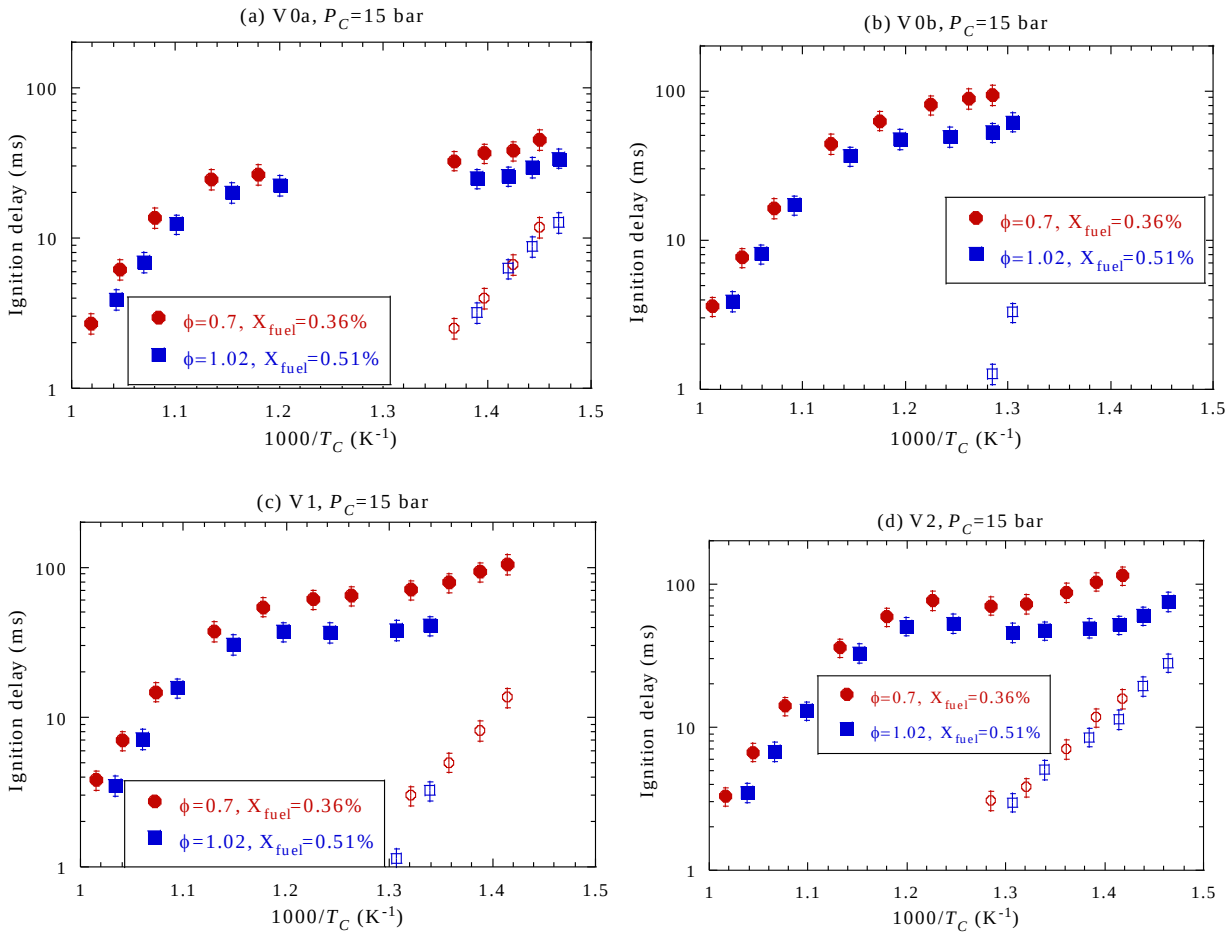

Figure 7: Effect of fuel loading on total and first-stage ignition delays at P_C=15 bar for (a) V0a, (b) V0b, (c) V1, and (d) V2. Filled symbols correspond to total ignition delays and open symbols correspond to first-stage ignition delays.

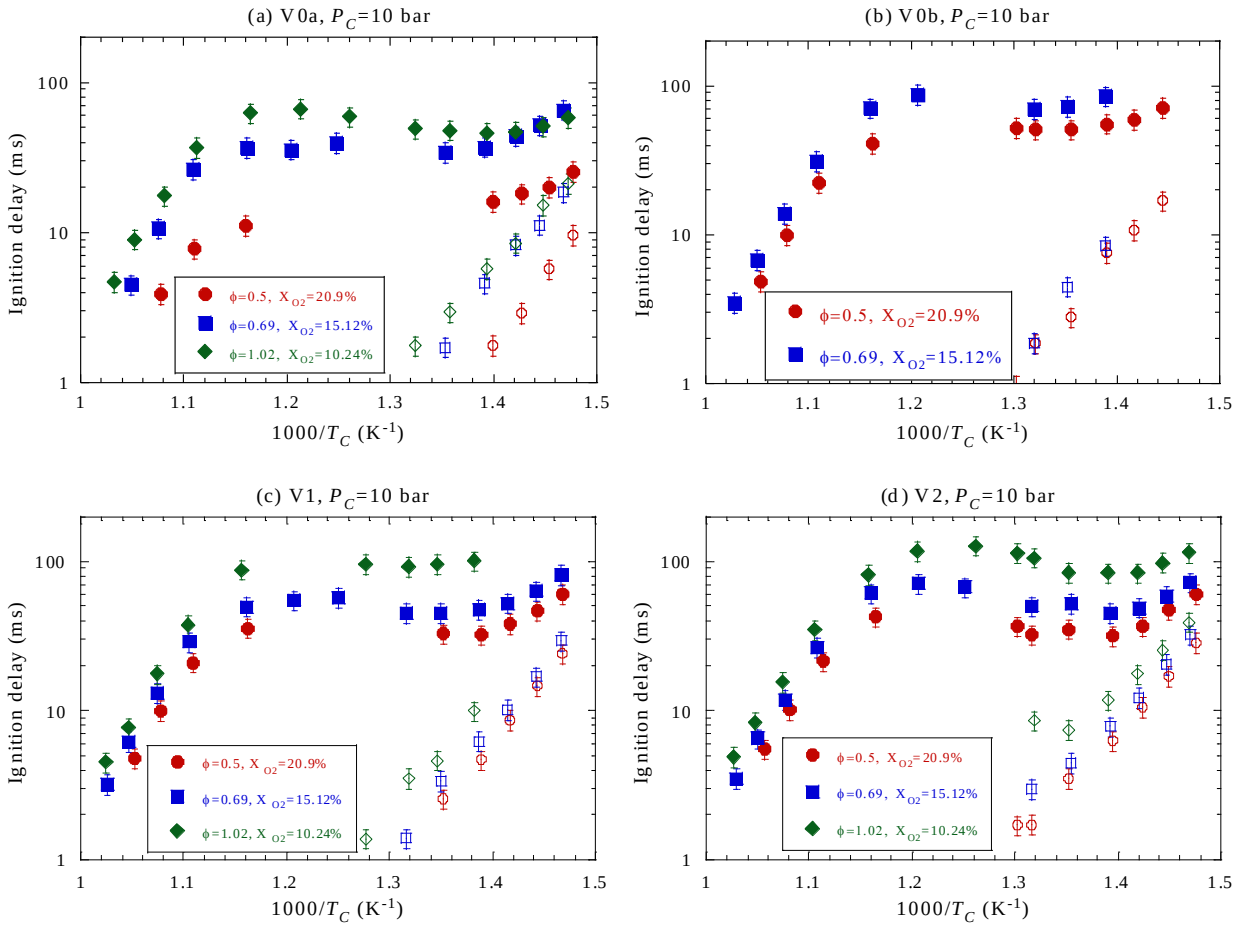

Figure 8: Effect of oxygen concentration on total and first-stage ignition delays at P_C=10 bar for (a) V0a, (b) V0b, (c) V1, and (d) V2. Filled symbols correspond to total ignition delays and open symbols correspond to first-stage ignition delays.

3.2 Autoignition Comparison of CRC Surrogates and CFA#2

Figure 9 compares the ignition delay results of the four CRC surrogates and CFA#2 under various experimental conditions listed in Table 2. According to the current result, it can be concluded that the discrepancies of total ignition delays of CFA#2 and CRC surrogates are more noticeable in the LTR and NTC regime, while their total ignition delays gradually overlap as temperature increases. Also, the overall ranking of total ignition delay times for CFA#2 and CRC surrogates are: V0b > V2 > V1 > CFA#2 > V0a. For the first-stage ignition delays, while the discrepancies are smaller compared to total ignition delays in the LTR, it can be observed that the first-stage ignition delays of V1, V2, and V0b are consistently longer than those of CFA#2 and V0a.

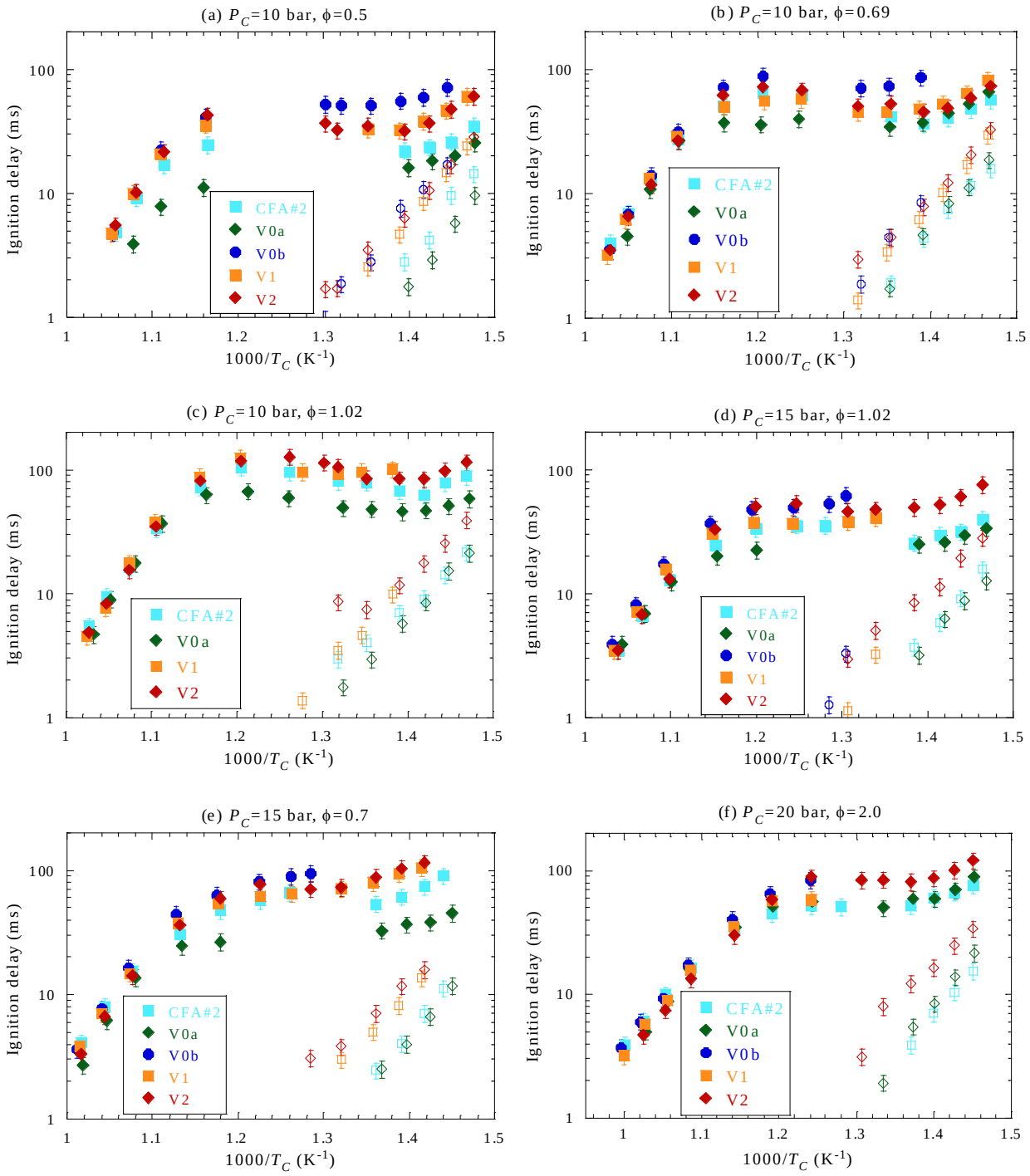

Figure 9: Autoignition results comparison of CRC surrogates and CFA#2 at all test conditions shown in Table 2. Filled symbols correspond to total ignition delays and open symbols correspond to first-stage ignition delays.

To further access how well the four CRC surrogates emulate the ignition response of CFA#2, their experimental pressure traces are compared with the same machine settings in RCM experiments. Figure 10 demonstrates these comparisons for representative pressure traces with the same machine settings in terms of number of shims and spacers used for varying geometric

compression ratio for ϕ=0.5 in air/P_C=10 bar, ϕ=0.7 with dilution/P_C=15 bar, and ϕ=1.02 with dilution/P_C=15 bar, respectively. Nonreactive pressure traces with the same test conditions and machine settings have also been shown in Figure 10 to substantiate that there is no exothermicity in the compression stroke and to demonstrate the extent of heat loss after the end of compression. It can be observed that with similar heat loss characteristics, the surrogate with a shorter total ignition delay has a higher post-ignition pressure rise. In terms of the peak pressure after hot ignition, V0a is about 15% higher than CFA#2, while V0b, V1, and V2 are comparable with CFA#2. This may be due to the multi-dimensional effects inside the reaction chamber that occur during the hot ignition process involving the exchange of mass and energy among the core region, the boundary layer, and the piston crevice [9]. These factors, coupled with the chemical reactions and heat release, could lead to different pressure and temperature rises after hot ignition for different fuels, with the most reactive V0a exhibiting the highest peak pressure.

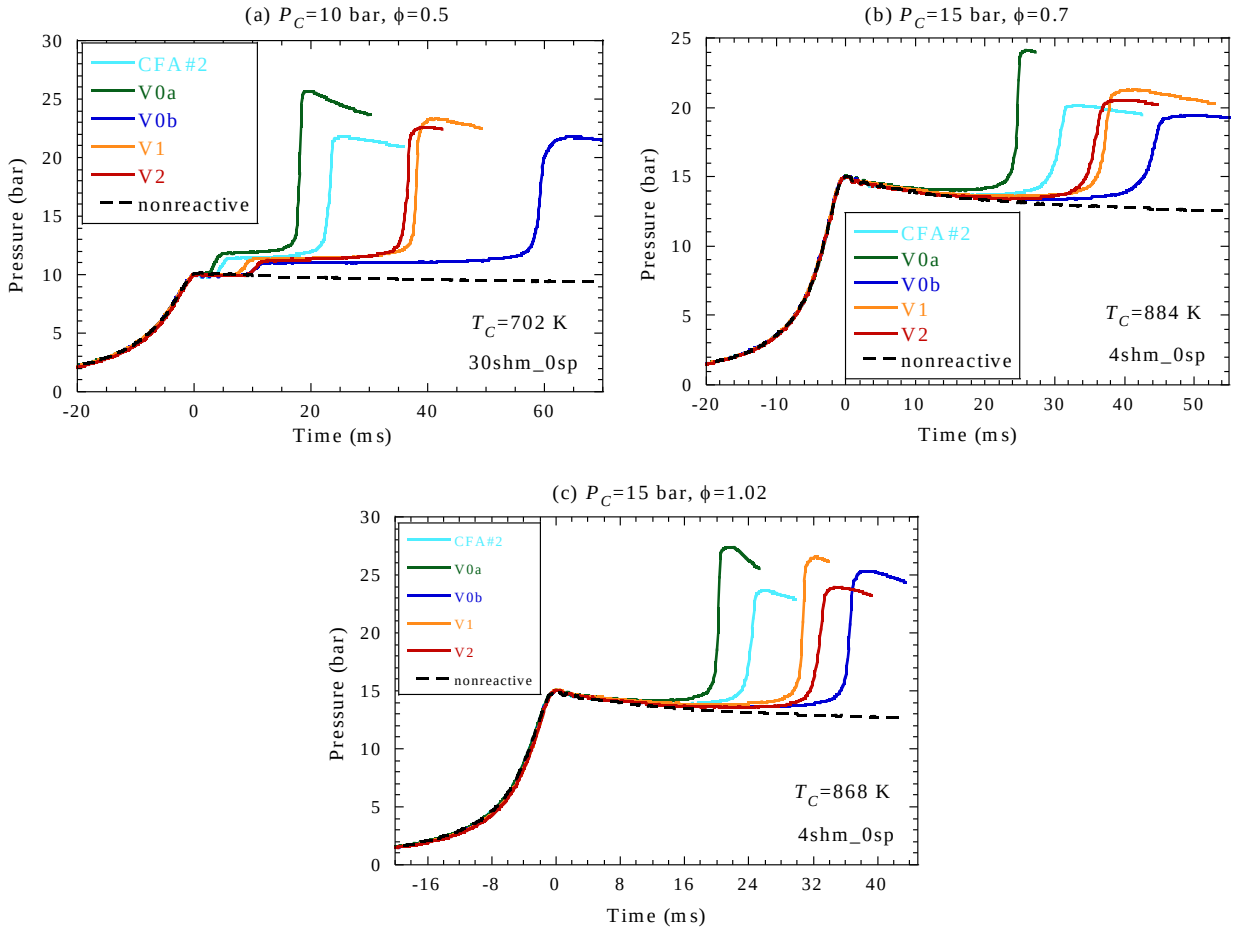

Figure 10: Plot showing the pressure trace comparison of CFA#2 and CRC surrogates under test conditions of (a) ϕ=0.5 in air/P_C=10 bar, (b) ϕ=0.7 with dilution/P_C=15 bar, and (c) ϕ=1.02 with dilution/P_C=15 bar.

4. Concluding Remarks

Autoignition of CRC diesel surrogates have been studied in a rapid compression machine at low-to-intermediate temperatures and elevated pressures. Vaporization checks have been conducted theoretically and experimentally before RCM experiments to ensure that there is no condensation inside the mixing tank. The effects of pressure, fuel loading, and oxygen concentration on total and first-stage ignition delay times were demonstrated for the four CRC surrogates. In addition, the ignition delay times of the four CRC surrogates have been compared with those of CFA#2 under various experimental conditions, with the discrepancies of total ignition delay times more noticeable in the LTR and NTC regime, and gradually overlap as temperature increases. Furthermore, the overall ranking of total ignition delay times for CFA#2 and CRC surrogates shows: V0b > V2 > V1 > CFA#2 > V0a, while the first-stage ignition delay times of V1, V2, and V0b are consistently longer than those of CFA#2 and V0a. These RCM results will be used to validate and refine chemical kinetic models of diesel fuels to predict combustion chemistry under engine relevant conditions for development of advanced diesel engines.

5. Future Work

(1) A chemical kinetic model of diesel surrogates is under development at Lawrence Livermore National Laboratory (LLNL).

(2) Manuscripts for journal publication consideration that document the current experimental results of CFA#2 and the four CRC surrogates, as well as the comparison of experimental data with the simulated results using the LLNL diesel surrogate model will be submitted to CRC for review and approval when ready.

6. List of Acronyms

CRC	Coordinating Research Council
IDT	Ignition Delay Time
ITR	Intermediate Temperature Regime
LLNL	Lawrence Livermore National Laboratory
LTC	Low Temperature Combustion
LTR	Low Temperature Regime
NTC	Negative Temperature Coefficient
RCM	Rapid Compression Machine

7. List of Figures

8. List of Tables

9. References

[1] G. Kukkadapu and C.J. Sung, Autoignition study of ULSD#2 and FD9A diesel blends, Combust. Flame 166 (2016) 45-54.

[2] M.P.B. Musculus, P.C. Miles, L.M. Pickett, Conceptual models for partially pre-mixed low-temperature diesel combustion, Prog. Energy Combust. Sci. 39 (2013) 246-283.

[3] C.J. Mueller, W.J. Cannella, J.T. Bays, T.J. Bruno, K. DeFabio, H.D. Dettman, R.M. Gieleciak, M.L. Huber, C.-B. Kweon, S.S. McConnell, W.J. Pitz, and M.A. Ratcliff, Diesel surrogate fuels for engine testing and chemical-kinetic modeling: Compositions and properties, Energy Fuels 30 (2016) 1445-1461.

[4] G. Mittal, C.J. Sung, A rapid compression machine for chemical kinetic studies at elevated pressure and temperatures, Combust Sci. Technol 179 (2007) 497-530.

[5] A.K. Das, C.J. Sung, Y. Zhang, G. Mittal, Ignition delay study of moist hydrogen/oxidizer mixtures using a rapid compression machine, Int. J. Hydrogen Energy 37 (2012) 6901-6911.

[6] D. Lee, S. Hochgreb, Rapid Compression Machines: Heat transfer and suppression of corner vortex, Combust. Flame 114 (1998) 531-545.

[7] P. Desgroux, L. Gasnot, L.R. Sochet, Instantaneous temperature measurement in a rapid-compression machine using laser Rayleigh scattering, Appl. Phys. B Laser Opt. 61 (1995) 69-72.

[8] C.J. Sung, H.J. Curran, Using rapid compression machines for chemical kinetics studies, Prog. Energy Combust. Sci. 44 (2014) 1-18.

[9] G. Mittal, M.P. Raju, C.J. Sung, CFD modeling of two-stage ignition in a rapid compression machine: assessment of zero-dimensional approach, Combust. Flame 157 (2010) 1316-1324.

10. Supplementary Materials

(1) "Ignition_Delay_Data_Diesel_Surrogates.xlsx": Tabulated RCM ignition delay data.

(2) "CFA#2_P_V_history.zip": Experimental pressure and volume traces of CFA#2 diesel.

(3) "V0a_P_V_history.zip": Experimental pressure and volume traces of CRC V0a surrogate.

(4) "V0b_P_V_history.zip": Experimental pressure and volume traces of CRC V0b surrogate.

(5) "V1_P_V_history.zip": Experimental pressure and volume traces of CRC V1 surrogate.

(6) "V2_P_V_history.zip": Experimental pressure and volume traces of CRC V2 surrogate.